Solid Oxide Fuel Cells 10, Nara, (2007), pp. 2049-2055.

Modeling of SOFC Anodes Based on the Stochastic Reconstruction Scheme

Yoshinori Suzue, Naoki Shikazono and Nobuhide Kasagi

Department of Mechanical Engineering, The University of Tokyo
Hongo 7-3-1, Bunkyo-ku, Tokyo 113-8656, Japan

A novel modeling scheme of SOFC anodes based on the stochastic structure reconstruction technique and the Lattice Boltzmann method (LBM) is proposed for performance assessment and optimization of anode microstructures. Cross-sectional microscopy images are processed to obtain phase-distinguished images (*i.e.*, Ni, YSZ and pore), and a three-dimensional model microstructure is reconstructed from the two-point correlation functions of the microscopy image. Then, the diffusivity, the electrical conductivity and the overpotential of the reconstructed anode are obtained through the LBM simulation. The electronic conductivity is predicted slightly smaller than the experimental result. However, the optimal sintering temperature is predicted to be around 1350 ºC, which is in good agreement with the literature data. Thus the proposed method predicts the anode performance for a given microstructure, and is considered as a promising tool for designing SOFC anodes.

INTRODUCTION

Solid oxide fuel cells (SOFCs) are considered to be the most powerful candidates for the future energy system, because of their high efficiency and fuel flexibility. Recently, performance improvement under lower temperature operation has been demanded for cost reduction and system durability. Anode porous microstructures are known to have significant effects upon the cell performance and durability of anode-supported SOFCs. Despite many experimental and numerical studies made so far, the optimization of anode microstructures still remains as a major issue. This is because the effects of anode microstructures on the anode performance are not fully understood.

Recently, the complete reconstruction of three-dimensional anode microstructures using the dual-beam focused ion beam-scanning electron microscopy was demonstrated by Wilson *et al.* (1). Although this method offers good understanding of microstructural features of SOFC anodes, the measurement and data processing time is a burden. On the other hand, the 3D structure estimation using the stochastic reconstruction scheme proposed by Yeong and Torquato (2) has been applied to various investigations on porous media because of its relatively low computational cost.

In this paper, anode 3D microstructures are reconstructed with the stochastic reconstruction scheme from the two-point correlation functions of 2D microscopy images. Then, the connectivity of each phase and the anodic overpotential of the reconstructed structures are obtained by using the Lattice Boltzmann method (LBM), and the effects of sintering temperature upon anode microstructures and cell performances are evaluated.

RECONSTRUCTION PROCEDURE

Sample Preparation

Composite anode samples were prepared from 8 mol % yttria-stabilized zirconia (YSZ, Seimi Chemical, Japan) and nickel oxide (NiO, Seimi Chemical, Japan). NiO and YSZ powders were mixed at the rate of 60:40 wt %, and the Ni-YSZ volume ratio resulted as 42.4:57.6. Cylindrical samples were prepared by extrusion molding (Kankyo Ceramics Research, Japan). These samples were pre-sintered at 1000 ºC for 3 h, and sintered for 3 h at 1300, 1350 and 1400 ºC, respectively, in order to investigate the effects of sintering temperatures. Then, sample anodes were reduced in 67 % H_2 with N_2 at 750 ºC for 10 h. The ramp rate was 10 ºC/min in all heating and cooling processes. A porosity of 1200 ºC-sintered sample was measured by a mercury porosimeter (Autopore IV9500, Shimadzu, Japan). The porosities of 1300, 1350 and 1400 ºC-sintered samples were extrapolated from their shrinkage ratios to be 0.450, 0.393 and 0.335, respectively.
After reduction, samples were infiltrated with epoxy to avoid smearing of soft Ni, and polished with a diamond paste. Cross-sectional images of polished samples were obtained with a confocal laser microscope (OLS3000, Shimadzu, Japan; 1024 pixel × 768 pixel, 1 pixel = 41 nm). The original microscopy images are shown in Fig. 1. Ni (white), YSZ (gray) and pore (black) can be clearly distinguished. Grain growth under high-temperature sintering was observed, especially for Ni.

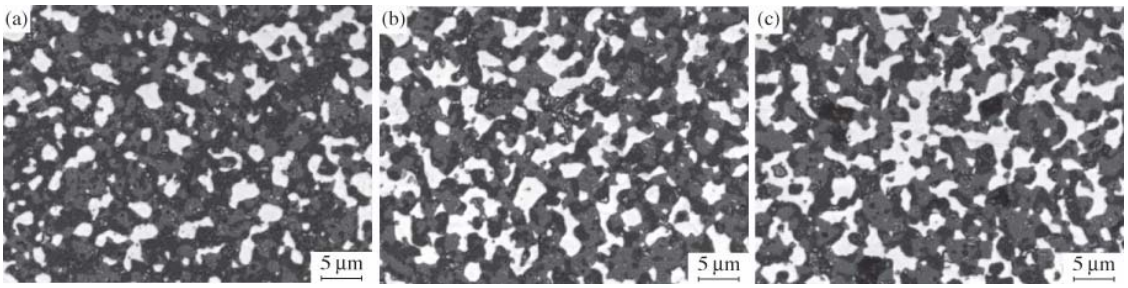

Figure 1. Cross-sectional microscopy images of samples sintered at (a) 1300 ºC, (b) 1350 ºC and (c) 1400 ºC.

Microscopy Image Modification

Three phases can be easily distinguished in raw images (Fig. 1) by using their luminance values (see Fig. 2). A differential filter was applied to sharpen grain boundaries. Then, each phase was differentiated so that the volume fractions in the 2D image match with the values calculated from the porosity and the NiO-YSZ mixing ratio. The phase-distinguished image of the 1400 ºC-sintered sample is shown in Fig. 3.

2D Image Analysis

From the phase-distinguished 2D images, the phase function, $Z(\mathbf{x})$, is defined at each pixel ($\mathbf{x}$).

$$Z(\mathbf{x}) = \begin{cases} 0 & \text{(pore,black)} \\ 1 & \text{(YSZ, gray)} \\ 2 & \text{(Ni, white)} \end{cases}. \qquad [1]$$

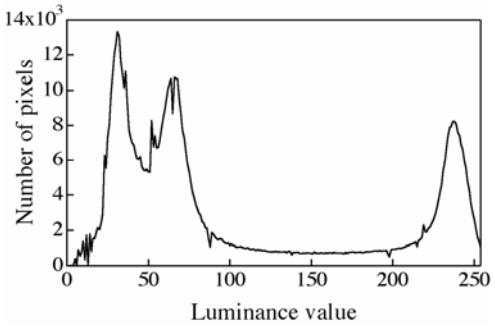

Figure 2. Luminance histogram of the 1400 ºC-sintered sample.

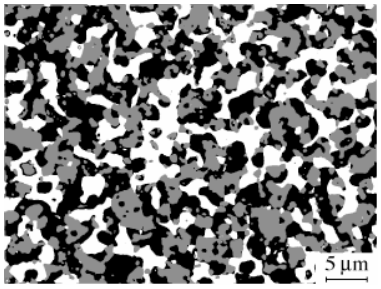

Figure 3. Phase-differentiated image of the 1400 ºC-sintered sample.

Using this phase function, the two-point correlation (or *probability*) function R_{ij} between phases i and j (i, j = 0-2) is defined as follows:

$$R_{ij}(r) = \frac{\overline{\delta(Z(\mathbf{x}),i)\delta(Z(\mathbf{x}+\mathbf{r}),j)}}{\overline{\delta(Z(\mathbf{x}),i)}}, \qquad [2]$$

where $\delta(i,j)$ represents the Kronecker's delta function. Figure 4 shows the two-point correlation curves of Ni-Ni and YSZ-YSZ. These correlation functions did not fully converge due to insufficient imaging areas, but these errors were relatively small (less than 5 %). As shown in Fig. 4, the YSZ-YSZ correlation seems to be more uniform than that of Ni-Ni, and this represents that YSZ grains are relatively well dispersed in cermet anodes. A slight increase of Ni-Ni correlations was observed for the separation distance around 3-4 μm, and this fact implies the existence of cluster-like structures of a size of 3-4 μm. As shown in Fig. 1, the high mobility of Ni resulted in this agglomeration of Ni.

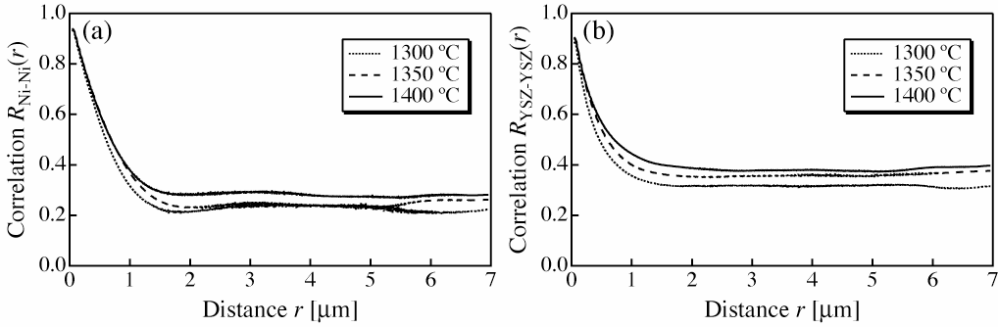

Figure 4. Temperature dependency of correlation functions of (a) Ni-Ni, (b) YSZ-YSZ.

Reconstruction Procedure

The 3D microstructure of a sample anode is reconstructed by the iterative scheme of Yeong and Torquato (2). The grid length l is 0.178 μm in each direction, and the whole computational domain size is 100 grids (17.8 μm in space) cubic. Periodic boundary conditions are imposed in all directions. At first, each voxel is assigned randomly with three phases according to the volume fractions. Then, reconstruction is carried out to minimize the cost function E defined as follows:

$$E = \sum_{i,j} \int_0^{r_0} \left\{ R_{ij}^{3D}(r) - R_{ij}^{2D}(r) \right\}^2 dr \,. \qquad [3]$$

Isotropic porous media are assumed, and the integral *dr* is performed only in the directions of the principal axes in order to reduce the computational load. The interval of integration r_0 was set as 7 μm.
Starting from a random configuration, two voxels of different phases are exchanged at each iteration step only when the cost function *E* decreases. The reconstruction is terminated after cost function remained constant for 100 Monte Carlo steps. Reconstructed 3D microstructures of three samples are shown in Fig. 5. Good reconstruction seems to be achieved with the residuals less than 1.0 %.

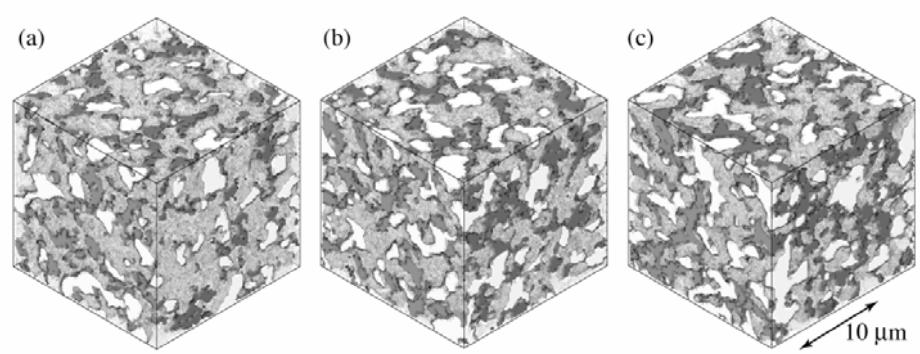

Figure 5. Reconstructed anode microstructures sintered at (a) 1300 ºC, (b) 1350 ºC and (c) 1400 ºC. White: Ni, gray: YSZ, transparent gray: pore.

PERFORMANCE CALCULATION SCHEME

Computational Modeling

In order to model the actual anode operating condition, current collector (CC) and YSZ electrolyte (EL) layers are added to the $x = 0$ and $x = 100l$ sides, respectively. The thicknesses of the CC and the EL layers are 1.78 μm ($10l$) and 3.56 μm ($20l$), respectively. For simplicity, binary gas composition of H_2/H_2O is assumed. Temperature is considered to be uniform. The standard calculation condition is summarized in Table I.

Table I. Standard simulation condition.

Fuel composition(H_2:H_2O)	Pressure	Temperature	Current density
80:20 (mol %)	1.0 atm	800 ºC	10000 A/m²

Constant and uniform current is assumed on the CC and EL boundaries. The local reaction current i_{reac} in the electrode is assumed to be proportional to the three-phase boundary length per unit volume (L_{tpb}), and the L_{tpb} is estimated to be 40 % shorter than the value directly calculated from the cubic voxel perimeter of the reconstructed structure. The Buttler-Volmer equation of Kawada *et al.* (3) is employed:

$$i_{reac} = i_0 L_{tpb} \left[\exp\left(\frac{2F}{RT} \eta \right) - \exp\left(-\frac{F}{RT} \eta \right) \right], \qquad [4]$$

where η is the overpotential $\phi_{el} - \phi_{io}$. The lineal exchange current density i_0 is defined from the patterned anode experiments of Bieberle *et al*. (4) as:

$$i_0 = 3.118 \times 10^{-2} \, p_{H_2}{}^{0.11} p_{H_2O}{}^{0.67} \exp\left(-\frac{10211}{T}\right). \quad [5]$$

Computational Scheme

The governing equations in pore, Ni and YSZ phases are the diffusion equation for hydrogen gas and the charge transfer equations for electron and ion, respectively. They are written as follows:

$$D\frac{\partial^2 C}{\partial x^2} = -\frac{RT}{2FP} i_{reac}, \quad [6]$$

$$\sigma_{el}\frac{\partial^2 \phi_{el}}{\partial x^2} = -i_{reac}, \quad [7]$$

$$\sigma_{io}\frac{\partial^2 \phi_{io}}{\partial x^2} = i_{reac}. \quad [8]$$

The LBM (5) is used to solve Eqs. [6]-[8] in each phase. The LB equation with the LBGK model in the collision term is written as follows:

$$f_i(\mathbf{x} + \mathbf{c}_i\Delta t, t + \Delta t) = f_i(\mathbf{x}, t) - \frac{1}{t^*}\left[f_i(\mathbf{x}, t) - f_i^{eq}(\mathbf{x}, t)\right] + w_i\Delta t. \quad [9]$$

In Eq. [9], f_i represents the density distribution function of gas, electron or ion with velocity $\mathbf{c}_i$ in the ith direction, and f_i^{eq} is the Maxewllian local equilibrium distribution. In this research, the D3Q6 model (i = 1–6) is used. The relaxation time t^* is 0.99 and fixed for all simulations. w_i in the RHS is a source term calculated from Eqs. [4]-[8]. A no-flux boundary condition is imposed on the boundary of each phase in the porous media by applying the halfway bounceback scheme.
Periodic boundary conditions are assumed in the spanwise (y and z) directions. At the CC surface, constant gas composition is assumed. Constant electronic and ionic current flux conditions are imposed on the CC and EL boundaries.

RESULTS

Evaluation of Network Connectivity

The volume fractions ε and the predicted tortuosity factors τ of reconstructed 3D structures are shown in Fig. 6. Usually, the tortuosity factor is used as a measure for describing the gas diffusivity in porous media. In the present study, the tortuosity factors are also applied to the electric conduction because of its simplicity to describe the network connection. The tortuosity factor τ of each phase is calculated using the effective diffusivity D_{eff} (or the effective conductivity σ_{eff}) obtained by the LBM simulations as follows:

$$D_{eff} = (\varepsilon/\tau)D, \quad [10]$$

$$\sigma_{eff} = (\varepsilon/\tau)\sigma. \quad [11]$$

Due to the stochastic and digitized calculation schemes in the reconstruction procedure, the volume fractions were slightly different from those calculated by the powder-mixing ratio and porosities, but these errors are negligible (less than 1 %). The tortuosity factors of solid phases decrease when the volume fractions become large; this means that good phase connection is achieved. The tortuosity factor of Ni at 1400 ºC is slightly lower than that of YSZ at 1300 ºC, while the volume fraction of 1400 ºC-sintered Ni is noticeably low. This is because the connection of Ni phase increases with sintering temperature. For validation, the Ni tortuosity measured by the four-probe conductivity test is also shown in Fig. 6(b). The predicted tortuosity factors are slightly larger than the experimental results. However, the temperature dependence of network connection can be reasonably well estimated by this scheme.

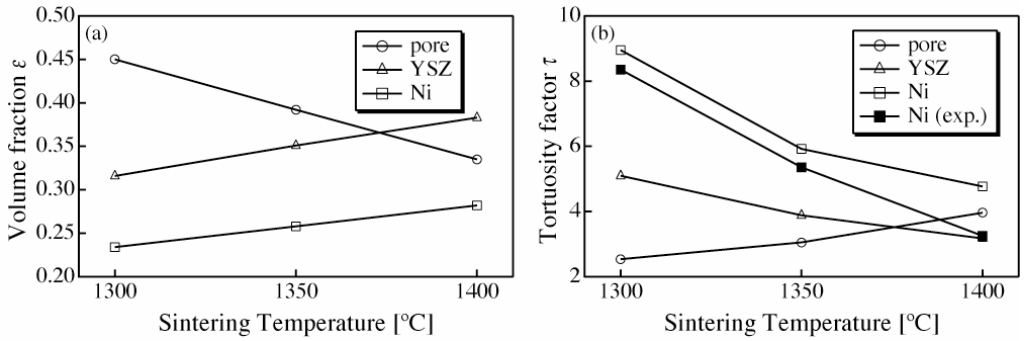

Figure 6. Temperature dependence of (a) volume fractions and (b) tortuosity factors.

Evaluation of Anodic Overpotential

The calculated anodic overpotential and the TPB densities (L_{tpb}) are shown in Fig. 7. The TPB density estimated by the random packing sphere model (6) is around 1.7-2.1 μm^{-2} under the present sample conditions. Thus, the reconstructed TPB densities are considered to be valid. From Fig. 7, it is found that the best anode performance is achieved by the 1350 ºC-sintered sample. This is attributed to the longer L_{tpb}. As described before, the best electronic and ionic network is achieved by the 1400 ºC-sintered sample. However, the electrochemical activity falls in the 1400 ºC-sintered sample due to the agglomeration of Ni. This result is in good agreement with the previous study (7).

Figure 8 shows the distribution of the activation overpotential of the 1350 ºC-sintered sample. It is found that the electrochemically active anode layer is very thin (~ 6 μm). This result is in good accordance with the 1D electrode simulation of Nam and Jeon (6), who used the similar Buttler-Volmer equation.

CONCLUSIONS

A novel modeling scheme of SOFC anodes based on the stochastic 3D structure reconstruction scheme and the LBM simulation is proposed and evaluated for the prediction of the effects of anode microstructures on the total anode performance. Cross-

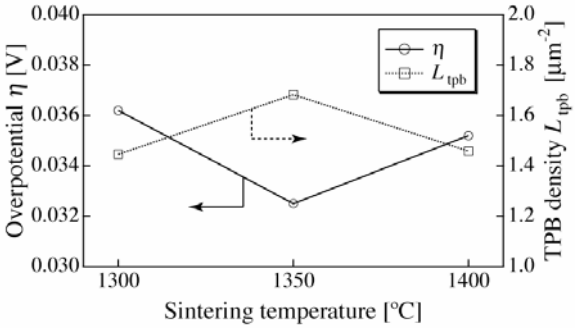

Figure 7. Temperature dependence of anodic overpotential and TPB density.

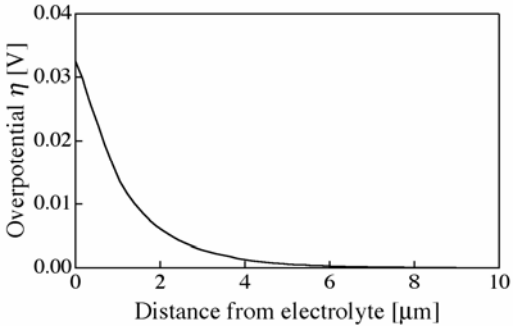

Figure 8. Activation overpotential distribution in the thickness direction.

sectional 2D microscopy images of anodes are processed to obtain phase-distinguished images, and 3D anode microstructure models are reconstructed from the two-point correlation functions of the 2D images. Good reconstruction is achieved by the present scheme, and residuals in two-point correlation functions are negligibly small. The diffusivity, the electrical conductivity and the overpotential of the reconstructed anode are obtained from the LBM simulation. Predicted tortuosity factors of Ni phase are slightly larger than the experimental data, but the present scheme is found to be able to predict the temperature dependence of the network connectivity qualitatively well. Furthermore, the anodic overpotential is calculated by coupling the mass and charge transfer and the electrochemical reaction. Finally, the effect of anode microstructures on the cell performance is discussed. It is found that the optimal sintering temperature should be around 1350 ºC, where a good ionic network and electrochemical activity are obtained. This result is in good agreement with the existing literature data, so that this scheme presently proposed is considered to be an effective tool to investigate the optimal anode microstructure.

Acknowledgements

This research was supported through the 21st Century COE Program, "Mechanical System Innovation," by the Ministry of Education, Culture, Sports, Science and Technology of Japan (MEXT). We would like to thank Professor Yuji Suzuki and Dr. Koji Fukagata at the University of Tokyo, Japan, for the beneficial advice and discussion. The authors also would like to thank Mr. Yu Yamaguchi and Mr. Yusuke Sakamoto at the University of Tokyo, Japan, for their cooperation in sample preparation and data acquisition.

References

1. J. R. Wilson *et al*., *Nature Materials*, **5** (2006).
2. C. L. Y. Yeong and S. Torquato, *Phys. Rev. E*, **58**, 1 (1998).
3. T. Kawada *et al*., *J. Electrochem. Soc*., **137**, 10 (1990).
4. A. Bieberle *et al*., *J. Electrochem. Soc*., **148**, 6 (2001).
5. S. Chen and G. D. Doolen, *Annu. Rev. Fluid Mech*., **30** (1998).
6. J. H. Nam and D. H. Jeon, *Electrochimica Acta*, **51** (2006)
7. T. Fukui *et al*., *J. Power Sources*, **110** (2002)